A Liquid Sensor Based on Frequency Selective Surfaces

Peter M. Njogu, Benito Sanz-Izquierdo, and Edward A. Parker

***Abstract*— A novel, simple and easy-to-fabricate liquid sensor using frequency-selective surfaces (FSSs) is proposed. The new sensor concept is based on modifying the capacitance between adjacent FSS elements when materials of different electrical characteristics are inserted. The change in capacitance produces a change in resonant frequency. The FSS design consists of a 9 × 9 array of square loops on 0.31λ × 0.31λ square unit cells with trenches between the loops. The trenches are filled with liquids under test (LTUs). The structure operates at 4.6 GHz without any liquid. When liquids are inserted in the trenches, the resonance frequency varies in relation to the dielectric constant of the liquid. This is observed by measuring the transmission coefficient (S_{21}). Butan-1-ol, ethanol, methanol, propan-2-ol, and xylene are used to demonstrate the sensing function. A maximum sensitivity of 8.65% for xylene was achieved. Furthermore, very low differences were observed between the measured and expected dielectric constant and loss tangent, thus validating the design. The device is inexpensive, compact, and easy to make and scalable for large-area operations in liquid detection for microwave sensing applications. This technique has potential applications in reconfigurable FSS.**

***Index Terms*— Dielectric, frequency-selective surface (FSS), liquid, material characterization, permittivity, sensor.**

I. Introduction

ANY material is characterized by its electrical properties in terms of complex permittivity and permeability. These can determine its electromagnetic response and its potential employment in specific industrial applications. Liquids are a type of material with a wide range of applications, including in the biomedical sector [1], [2]. The methods for sensing and determining the electrical properties of liquids are continuously evolving [3].

Microwave sensors have gained popularity due to their simplicity, inexpensive fabrication, and ease of use. One widespread technique is to use a resonating structure for determination of complex permittivity of the material. They operate on the principle of measuring the complex permittivity through analysis of the fundamental resonance frequency shift in the transmission/reflection response. At single or discrete set of frequencies, resonant technique offers the potential for accurate measurements. Waveguide, dielectric, and coaxial cavity resonators have traditionally been employed for materials characterization [4], [5]. The material to be characterized is inserted in the cavity location where the electric field is at its maximum causing cavity perturbation. The introduction of material results in changes in the resonant frequency of the cavity [3]. Exploiting this phenomenon, several sensing devices have been developed. In [6], a planar substrate integrated waveguide cavity resonator is presented where microfluidic capillaries are used for the insertion of the material. This method is also employed in [7] and [8] with the implementation of a split-ring resonator with a microfluidic channel. The split-ring and capillary concepts are combined in [9] where a complementary split-ring resonator (CSRR) is presented for dielectric characterization of liquids. This is further developed in [10] where an open complementary split-ring resonator is employed with a slot container. In [11], dual mode, quarter ring microstrip resonators microfluidic sensor with capillary are used. In [12], a sensor that exploits the excitation of a resonant mode within a cavity containing a minute sample of a liquid is presented. In [13], an RFID sensor is presented for identification and evaluation of liquid chemical based on the shift in the resonant frequency of an applied UHF RFID chipped tag.

Metamaterials are artificially constructed composites that exhibit electromagnetic properties that are difficult to achieve using conventional or naturally occurring materials [14] and include electromagnetic bandgap (EBG) structures [15] and FSS [16]. They have recently been used for sensing liquids. In [17], [18], and [19], metamaterial absorber sensors are proposed where an air gap between a copper plate and backside resonator is used to fill chemicals' liquids. EBGs have recently been employed in wireless sensor design in [20] by creating trenches between adjacent cells. This concept was advanced in [21] using a Casero Fractal design element.

In general, these liquid sensors provide good sensitivity and accuracy, but they also present design and operational complexities, and bulkiness, while others are delicate and require intricate assembly. Their design structure requires complicated measurement setups followed by complex design construction. Further costs accrue due to additional drilling and cutting for microfluidic subsystems. Extra parts, e.g., capillaries, capsules, and liquid containers, would then be needed, which further increases the costs. Others EBG-based [20], [21] are two parts designs, which must be intricately assembled beside

Manuscript received 17 May 2022; revised 25 August 2022; accepted 24 October 2022. Date of publication 9 November 2022; date of current version 19 January 2023. This work was supported in part by the EPSRC grant titled Low-Profile Ultra-Wideband Wide Scanning Multi-Function Beam-Steerable Array Antennas under Grant EP/S005625/1 and in part by the Royal Society-International Exchanges 2019 Cost Share (NSFC) under Grant IEC\NSFC\191780. *(Corresponding author: Peter M. Njogu.)*

The authors are with the School of Engineering and Digital Art, University of Kent, CT2 7NZ Canterbury, U.K. (e-mail: pmn20@kent.ac.uk; b.sanz@kent.ac.uk; e.a.parker@kent.ac.uk).

Color versions of one or more figures in this article are available at https://doi.org/10.1109/TAP.2022.3219540.

Digital Object Identifier 10.1109/TAP.2022.3219540

the design complexity. A single unit, which is easy to make and use sensor, implies simplicity, lower cost, and ease of assembly.

Frequency-selective surfaces (FSSs) are electromagnetic filtering structures usually consisting of arrays of periodic conductors [22], [23] on a supporting dielectric material. They are a type of metamaterial [24]. FSSs modify the incoming electromagnetic signal in relation to their instrinsic resonant frequency. Their responses are dependent on the geometry and spacing of the element, dielectric material thickness, and properties as well as that of its surroundings [23]. This property can be used to develop contactless sensors. FSS sensors have been designed to monitor structural health [25], [26], and [27], sensing of temperature and strain [28], breathing [29], strain [30], and dielectric characterization [31], [32].

In this article, an FSS-based sensor for sensing liquids falling onto a surface is proposed. In the new concept outlined in this work, the sensing function is achieved by altering the capacitance between adjacent FSS elements when materials of different electrical characteristics are inserted in trenches. The change in capacitance produces a change in the frequency resonance, which is detected as transmission response of the FSS. Trenches were dug in the dielectric around the conductors. The basic principle of operation of the proposed sensor is the excitation of a resonant mode of the FSS with the trenches filled with different liquids under test (LUTs). The FSS sensor operates at about 4.6 GHz with a broad range of frequencies in relation to the LUT. To the best of the authors' knowledge, this is the first design based on the FSS structure for sensing of liquids. The proposed sensor is scalable and can be redesigned to operate in different frequency bands. The motivation is the creation of a wireless sensor for the detection of liquids falling into a surface. The main application is on the detection on medium-to-large surfaces that can be adjusted by the array size. A curve-fitting approach is employed to estimate the LUT complex permittivity and sensitivity analysis based on the shifted parameters. The rest of this article is organized as follows. Section II details the geometry of the unit cell, the integrated trenches, and its characteristic behavior. Section III details the fabrication and measurements of the design, while Section IV discusses the performance evaluation of the proposed sensor. Finally, Section V discusses the conclusion.

II. FSS Sensor/Detector Design

A. FSS Sensor Unit Cell Design

The FSS was designed, simulated, and tested using CST Microwave Studio[1]. For simplicity, the FSS was simulated as an infinite structure using a unit cell with periodic boundaries. Fig. 1(a) shows the geometry of the unit cell of the FSS sensor design. A band stop FSS was selected as changes in the sensors could be observed through nulls in the transmission responses. In terms of element, a square loop FSS was used because it offers dual polarization and good angle of incidence behavior.

In the design, the square loops were made of copper and the substrate was RT/Duroid 5880 of thickness 3.175 mm,

[1]Trademark.

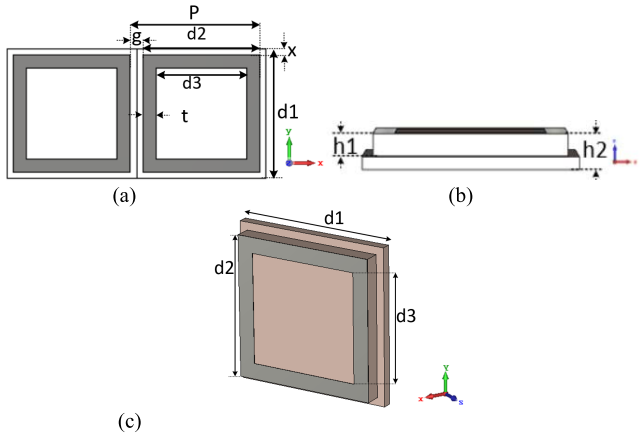

Fig. 1. (a) Top view and dimensions of the FSS cell. (b) Cross-sectional view. (c) Perspective view.

TABLE I
Unit Cell Dimensions

Parameter	d_1	d_2	d_3	P	g	x	t	h_1	h_2
Value (mm)	20	18	14	20	2	1	2	2	3.175

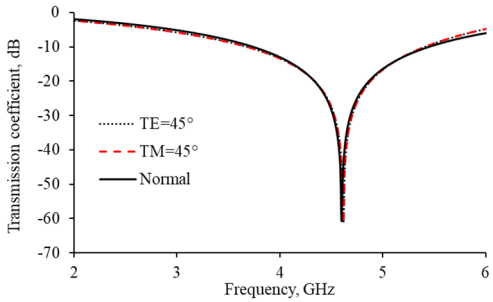

Fig. 2. Simulated transmission responses of the loop FSS.

dielectric constant ε_r of 2.2, and loss tangent (tan δ) of 0.0009. The cell had 1 mm wide and 2 mm deep trenches around its edges. The trenches were introduced through the partial removal of the substrate around the square loop, as shown in Fig. 1(b). The trenches reduce the amount of dielectric material, which decreases the permittivity and losses of the FSS in free space. The unit cell and the square loop dimensions were optimized to operate at 4.6 GHz. The gap $\times$ between the conductor loop and the edge of the unit cell is 1 mm. The periodicity, P, of the square loop array is the sum of g, the gap between adjacent loops, and d_2, the length of the conductor. d_1 is the length of the unit cell element. The design dimensions are shown in Table I. Fig. 2 shows the simulated transmission response of the FSS for angle of incidence at 0° incidence, 45° TE, and 45° TM incidence. TE denotes the E-plane response, whereas TM denotes the H-plane response. Resonance of the unit cell occurred at normal incidence with a frequency of 4.6 GHz with no appreciable frequency drift at TE 45° and TM 45°, i.e., 45° off broadside illumination for TE and TM polarization.

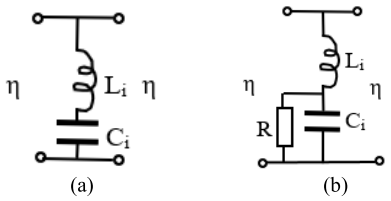

Fig. 3. EC models: (a) square loop FSS and (b) FSS with a lossy liquid in the trenches.

B. Square Loop Operations and Equivalent Circuit (EC)

The square loop FSS has band reject frequency response dependent on its physical dimensions [33]. It is a relatively simple shape and ideal to build a prototype for performance assessment or application. The EC of the square loop FSS has been investigated in [34], [35], and [36]. Fig. 3(a) presents the EC of the square loop band stop filter. The EC model provides a simple and fast method of FSS analysis that is supported by transmission line analogy in which equivalent capacitive (C_i) and inductive (L_i) lumped components construct of the FSS can be calculated. η is the characteristic intrinsic impedance of free space equal to 377 Ω. The proposed FSS array is symmetrical with periodicity P and a gap g between two adjacent conductor loops. It can be represented as lumped elements consisting of capacitance (C_i) and inductance (L_i). Gap g represents the capacitive elements, while the length of the conductor represents the inductive element. Resonance occurs when the perimeter of the loop is approximately one wavelength. The inductance and capacitance values determine the resonance frequency ω as

$$\omega = \frac{1}{\sqrt{L_i C_i}} \tag{1}$$

The dielectric material affects the reflection or transmission responses. With a finite thickness, the dielectric material effect on the FSS structures can be explained using the EC analysis. The designed inductive FSS is a square loop of width t. Its intrinsic capacitance C_i and inductance, L_i, for TE incident wave can be approximated from path capacitance and strip inductance using (2) and (5), respectively, a conducting strips approximation developed by [37] that enables the calculation of L_i and C_i values. For transverse electrical (TE) incidence wave, the vertical strips of the FSS act as a L_i impedance in the EC and the horizontal gratings as a C_i impedance [33] of

$$Ci = \frac{2\mathrm{P}}{\eta\pi c}\left\{\mathrm{In}\left(\mathrm{cosec}\left(\frac{\pi g}{2\mathrm{P}}\right) + G(\lambda, g, \mathrm{P})\right\}\right. \tag{2}$$

where C_i is the intrinsic capacitance between adjacent loops, determined by periodicity P and the gap g between adjacent loops. $G(\lambda, g, \mathrm{P})$ is a correction term expressed by

$$G=\left\{\frac{Q_2\cos^4\left(\frac{\pi g}{2\mathrm{P}}\right)}{1+\mathrm{Q}_2\sin^4\left(\frac{\pi g}{2\mathrm{P}}\right)} + \frac{1}{16}\left(\frac{\mathrm{P}}{\lambda}\right)^2\left(1-3\sin^2\left(\frac{\pi g}{2\mathrm{P}}\right)\right)^2\cos^4\left(\frac{\pi g}{2\mathrm{P}}\right)\right\} \tag{3}$$

and the factor Q_2 is given by

$$Q_{\mathrm{n}} = \frac{1}{\sqrt{1-\left(\frac{2\mathrm{P}}{\mathrm{n}\lambda}\right)^2}} - 1 \tag{4}$$

where the value of n in this case is 2.

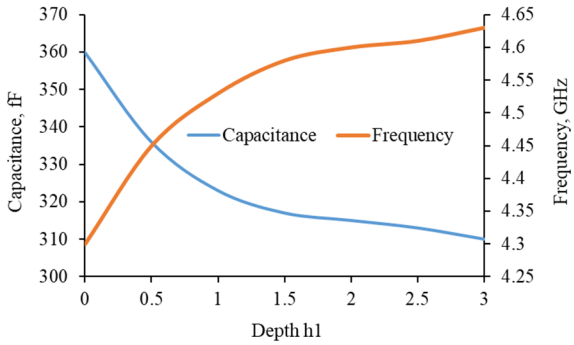

Fig. 4. Plot of capacitance and frequency versus the trench depth.

To approximate the strip inductance, L_i, g in the correction term (3) is substituted by t, and L_i results in

$$L_i = \frac{\eta\lambda^2}{32\mathrm{P}\pi\,\mathrm{c}\left\{\ln\left(\mathrm{cosec}\left(\frac{\pi t}{2\mathrm{P}}\right) + \mathrm{G}(\lambda, t, \mathrm{P})\right)\right\}} \tag{5}$$

where L_i is the strip inductance determined by conductors of periodicity P, width t, c is the speed of light, and η is the impedance of free space.

From (1) and (5), the theoretical component values for free-standing FSS are $L_i = 3.8114$ nH and $C_i = 214.26$ fF. This capacitance needs to be adjusted due to the effect of dielectric. In a one-sided substrate, the capacitance increases proportional to the effective relative permittivity [23], [38] given by

$$\varepsilon_{eff} = \frac{\varepsilon_r + 1}{2}. \tag{6}$$

Although (6) is a general equation for the cases when the substrate is sufficiently thick ($>\lambda/5$) [33], it can be a good approximation in the case of square loops even in substrates of thicknesses of about 0.05λ [39]. Therefore, using (6), the resulting capacitance when compensated by the dielectric substrate is $C_i = 342.9$ fF. The resonant frequency for this LC circuit is approximately 4.5 GHz, which is within the expected 5% error margin of the frequency of 4.3 GHz for the FSS obtained from the simulation of the dielectric-loaded FSS (no trenches).

In liquid sensing, the dielectric losses of the liquids in the trenches can be high. These losses can be represented as a resistor in parallel with the capacitor, as shown in Fig. 3(b).

C. Parametric Analysis

Parametric study was conducted to determine the behavior of the FSS for varying empty trenches' depth (h_1), from 0.0 to 3.0 mm, at 0.5 mm intervals. Fig. 4 shows the effect of changing trench depth (h_1) on resonant frequency and the corresponding capacitance. In our model, the inductance is constant ($L_i = 3.8114$ nH) [22]. The capacitance has been calculated using the frequency obtained in simulations and (1). As expected, removing dielectric material decreases the effective permittivity and capacitance and increases the resonant frequency. The capacitance as a function of depth, h_1, follows the fit equation:

$$C_i = -3.7778h_1^3 + 25.143h_1^2 - 58.103h_1 + 359.76 \text{ fF}. \tag{7}$$

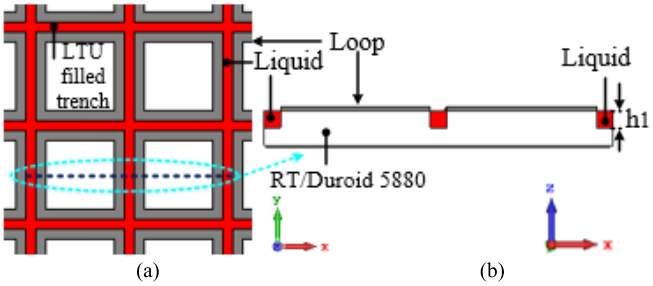

Fig. 5. (a) Top view and (b) cross-sectional view of a section of the FSS sensor liquid-filled trenches.

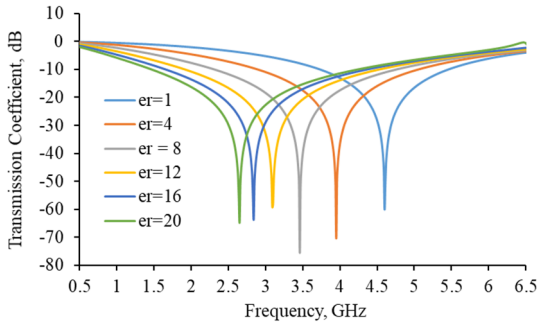

Fig. 6. S_{21} of the FSS with liquid of various e_r in the trenches.

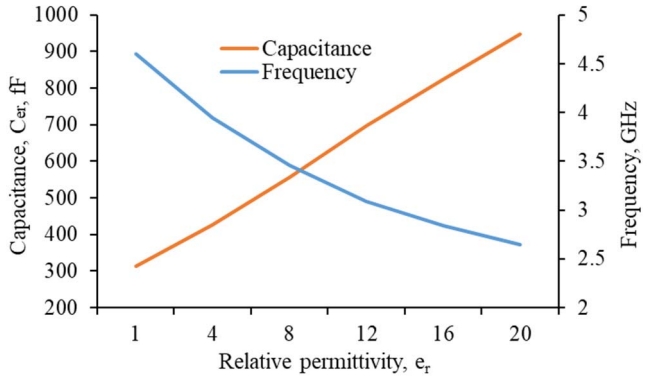

Fig. 7. Permittivity e_r versus frequency and capacitance.

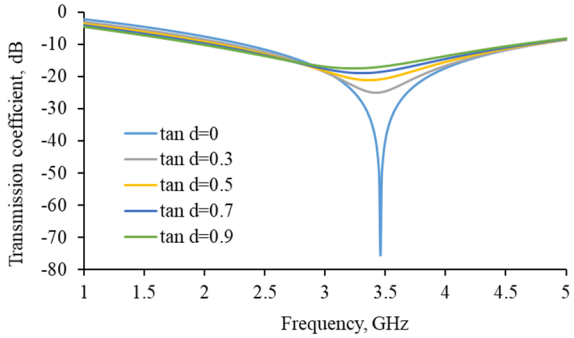

Fig. 8. Simulated dependence of transmission coefficient (S_{21}) of the FSS loss tangent (tan δ) of the liquid in the trenches ($\varepsilon_r = 8$).

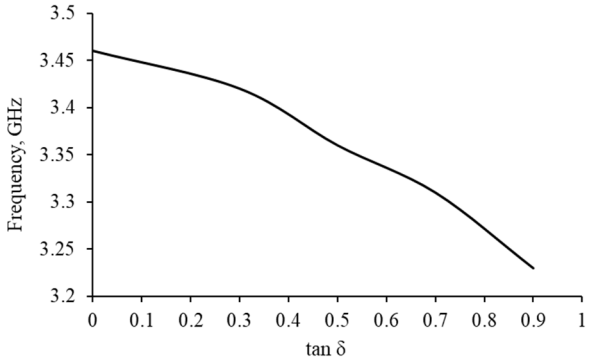

Fig. 9. Sensitivity of the FSS structure: simulated dependence of the resonant frequency on loss tangent (tan δ).

TABLE II
ELECTRICAL CHARACTERISTICS OF THE LUTS

Liquid	Relative permittivity ε_r	Loss tangent (tan δ)
Butan-1-o1	3.29	0.47
Propan-2-o1	3.8	0.64
Ethanol	5.08	0.96
Methanol	12.42	0.65
Xylene	2.57	0.018

To assess the potential behavior of the proposed FSS structure (see Fig. 1) as a liquid sensor, a simulation was carried with the trenches filled with materials of various dielectric constants and loss tangents. Fig. 5 shows the FSS structure indicating the sections of the design with liquid. In the initial study, shown in Figs. 6 and 7, the dielectric permittivity was varied from 1 to 20, and the loss tangent was fixed at 0. The resonant frequency decreased with increase of the dielectric constant. From (1), capacitance C_i due to liquids of varying ε_r values in the trenches was obtained and is also shown in Fig. 7. C_i increases linearly with ε_r as

$$C_i = 33.312\varepsilon_r + 288.89 \text{ fF}. \tag{8}$$

The effect of changes in loss tangent on the transmission response and resonance frequency is shown in Figs. 8 and 9, respectively. The permittivity of the liquid was kept at 8, while the loss tangent was varied between 0 and 0.9.

The depth of the null in the transmission coefficient curve decreases with the increase in loss tangent. A small decrease in resonant frequency is also observed, with a maximum of about 6% shift for a value of tan δ of 0.9.

D. Sensor Study for Readily Available Liquids

Five chemical liquids were used to authenticate the sensing/detecting functionality of the proposed design. These were Butan-1-o1, Propan-2-o1, ethanol, and methanol whose dielectric properties at 5 GHz and 20 ° were obtained from [40] and xylene from [41] and are shown in Table II. Fig. 10 shows S_{21} of the unit cell elements when the trenches are filled with the different LUT.

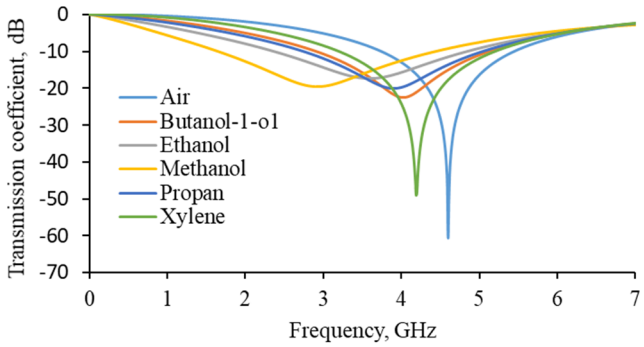

Fig. 10. Simulated frequency response of the proposed sensor structure for the various LUT.

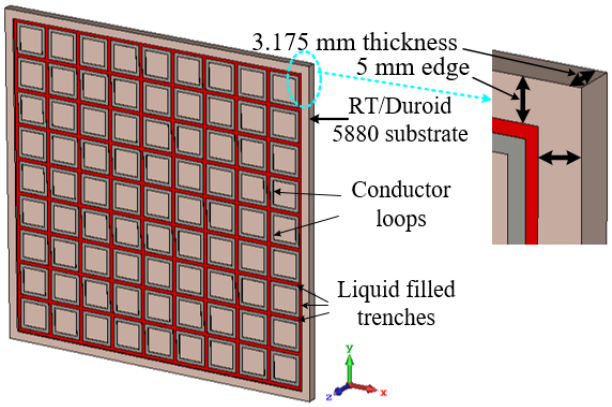

Fig. 11. Perspective view of the FSS sensor prototype with liquid-filled trenches.

III. Fabrication and Measurements

A. Fabrication

The FSS unit cell with dimensions as in Fig. 1 and Table I was extended to a 9 × 9 array to create a prototype of the sensor. The model of the sensor is shown in Fig. 11 with the liquid-filled trenches depicted in red. It has a 5 mm wide edge to hold the liquids inside and for mechanical purposes, making a total dimension of 192 × 192 mm. The prototype was fabricated at Printech Circuit Laboratories [42] using standard printed circuit board (PCB) procedures. It was then milled using a high-precision milling machine to create the trenches around the loops. The fabricated sensor is shown in Fig. 12(a) while Fig. 12(b) shows the milled trenches.

B. Measurements and Results

Using a Marconi Instruments microwave test set 6204B and in a plain wave chamber, the insertion loss of the FSS was measured with empty trenches. Fig. 12(c) shows the measurement setup. The trenches were then filled using a syringe with the correct amount of liquid (14 mL) and the transmission response (S_{21}) measured. The FSS structure was kept horizontal using a bubble level to ensure that the liquid was uniform throughout the structure. The S_{21} results are shown in Fig. 13. Table III tabulates both the simulated and measured resonance frequency (f_s) and the frequency shift

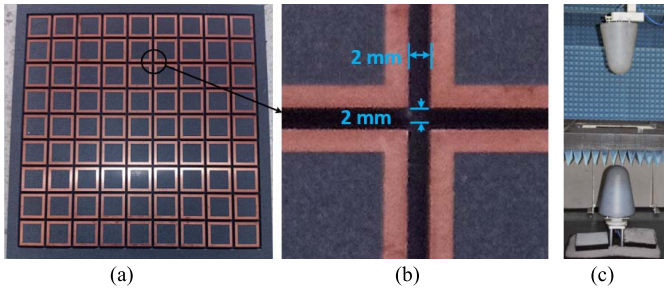

Fig. 12. (a) Fabricated FSS sensor. (b) Empty trenches. (c) Measurement setup.

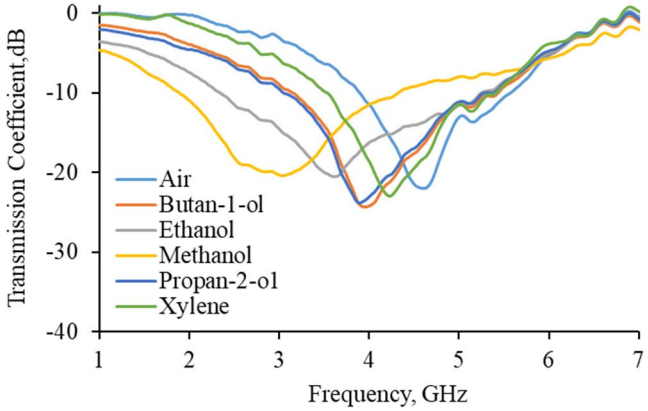

Fig. 13. Measured frequency response of the proposed sensor structure for various LUTs.

TABLE III
MEASURED RESONANCE FREQUENCY AND FREQUENCY SHIFT

LUT	f_s GHz		Δf GHz	
	Simulated	Measured	Simulated	Measured
Butan-1-o1	4.02	3.92	0.58	0.68
Ethanol	3.59	3.61	1.01	0.99
Methanol	2.92	3.01	1.68	1.59
Propan-2-o1	3.9	3.83	0.7	0.77
Xylene	4.19	4.24	0.41	0.36

(Δf) from the reference of the LUT. The resonance frequency for both the simulated and measured shows the frequency shift toward lower frequencies from the reference frequency, i.e., air resonance. This agrees with similar observations in [43] and [44]. The resonance points shift to the lower frequencies when the trench is filled with liquids of high dielectric constant. The differences between simulated and measured results could be due to fabrication errors, potential loss of liquid when inserting into the trenches, quality of the LUT, and possible differences in the permittivity values of LUT from those given in [40].

IV. Proposed Sensor Performance Evaluation

A. Sensitivity Analysis

The proposed design performance evaluation was conducted with the integrated fluidic trenches on the FSS filled with the five different liquids of different electrical properties described in Section II. The sensitivity (S) as a performance parameter

TABLE IV
MEASURED PERFORMANCE ANALYSIS OF SENSOR

LUT	Resonance Frequency (GHz)	Frequency Shift (GHz)	Sensitivity (%)
Air	4.6	-	-
Butanol-1-o1	3.92	0.68	7.58
Ethanol	3.61	0.99	6.72
Methanol	3.01	1.59	4.63
Propan-2-o1	3.83	0.77	7.18
Xylene	4.24	0.36	8.65

was used to evaluate the sensor performance according to the criterion proposed in [21] and [44]. To estimate the sensitivity (S) of the device, air-filled trenches were chosen as the reference. The proposed criterion gives the mathematical expression of the sensitivity, S, of

$$\mathrm{S} = \frac{\Delta f / f_s}{\Delta \varepsilon} \tag{9}$$

Δf is expressed as $(f_o - f_s)$, where f_o and f_s are the resonance frequency of the FSS when filled with air and the LUT, respectively. $\Delta\varepsilon$ is $(\varepsilon_s - \varepsilon_o)$, where ε_s and ε_o are dielectric constants of the LUT in the trench and air, respectively. Table IV shows the frequency shift and the computed sensitivity (S) of the various LUTs.

B. Material Dielectric Characterization

The complex permittivity (ε_r) and loss tangent (tanδ) of the LUT were calculated using mathematical models derived using the polynomial curve-fitting technique [2] and [21]. The necessary equations that best fit the given data set were generated to a 3° for greater accuracy. The resonating frequency (f_s) and bandwidth of frequency shifting (Δf) were used to determine the dielectric constant and loss tangent of the LUT, respectively, to a good degree of accuracy. The relationship between the resonating frequency variations with respect to the change in the dielectric values of LUT was expressed using the third-order polynomial expression

$$\varepsilon_r = -1.6763 f_s^3 + 24.8613 f_s^2 - 121.5387 f_s + 198.7187 \tag{10}$$

where ε_r is the calculated real permittivity and f_s is the LUT resonating frequency. The relationship between the bandwidth of frequency shifting and loss tangent (tan δ) was mathematically derived as a third-order polynomial as the best fit of the given dataset and is expressed by

$$\tan\delta = -2.0252\Delta f^3 + 4.3111\Delta f^2 - 1.3509\Delta f + 0.0395 \tag{11}$$

where tan δ is the calculated loss tangent and Δf is the LUT frequency shift from the reference.

From (8) and (9), the dielectric constant and loss tangent of samples of LUT of unknown permittivity and loss tangent were calculated and compared to the actual published values to validate the data. The calculated values of ε_r and tan δ are shown in Table V. The calculated results demonstrate a good agreement with actual permittivity and loss tangents values of all the LUT. The root-mean-square error between the actual and the calculated permittivity and the loss tangent was also calculated. The highest error of 1.7% and 3.3% for dielectric tangent and loss tangent, respectively, validates the performance of the device. The error could be due to the scattering parameters of the microwave sensor being influenced by the electric and magnetic properties of its surroundings, which can be reflected in the insertion loss S_{21} of the resonator. Impurities and analytes in the trench can have an effect on the amplitude tab3

TABLE V
CALCULATED DIELECTRIC PROPERTIES OF THE LUT

LUT	Dielectric constant (εr)			Loss tangent (tan δ)		
	Actual	Calculated	RMS Error (%)	Actual	Calculated	RMS Error (%)
Air	1	-	-	-	-	-
Butanol-1-o1	3.29	3.3416	1.6	0.47	0.4776	1.6
Ethanol	5.08	5.0959	0.31	0.96	0.9624	0.25
Methanol	12.42	12.4189	0.009	0.65	0.6498	0.03
Propan-2-o1	3.8	3.7357	1.7	0.64	0.6308	1.4
Xylene	2.57	2.5651	0.19	0.018	0.0174	3.3

*Root mean square (RMS) computed as $\frac{\sqrt{(Actual-Calculated)^2}}{Actual}$

TABLE VI
COMPARISON OF THE PROPOSED DESIGN WITH THE REPORTED METAMATERIAL-BASED SENSING DESIGNS

Parameter	[21](EBG)	[20] (EBG)	This work (FSS)
Resonant Frequency (GHz)	2.45	2.45	4.6
Construction	Complex	Complex	Simple
Maximum Measured Sensitivity	0.875	-	8.65
Minimum frequency shift Δf (GHz)	0.054	-	0.68

V. DISCUSSION AND CONCLUSION

A new concept for microwave liquid sensors based on FSS has been demonstrated. The sensor uses trenches between FSS elements to modify the transmission response when liquids with different permittivity are inserted. A mathematical model was developed for determination of the dielectric constant and loss tangent of the LUT. The evaluated complex permittivity and loss tangent are in good agreement with the actual values. The highest errors in the measured values of the dielectric constant and dielectric loss are within 1.7% for Propan-2-o1 and 3.3% for xylene, respectively. This demonstrates that the proposed microwave sensor is suitable as a low-cost platform for the detection of liquids with good sensitivity and low detection error. Table VI summarizes the performance analysis of the reported metamaterial EBG detectors closest to the proposed design. It shows that, besides its simplicity, it offers higher sensitivity and thus improved the detection performance.

The developed sensor is ideal for instances requiring robust, real-time monitoring at low cost and complexity, low power

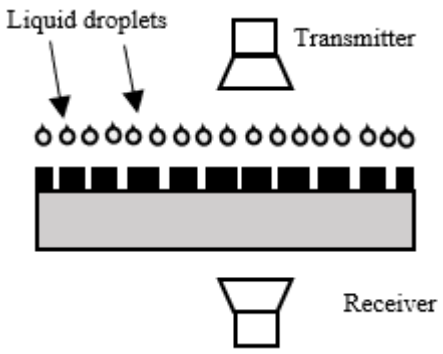

Fig. 14. Illustrative potential FSS sensor application.

consumption, and simple fabrication techniques. The independent resonant nature due to each chemical allows the device to be reused for different and various liquids. The contactless nature of the detection process makes it suitable for a safe working environment. For example, it can be used in industrial processes where dangerous chemicals may need to be identified. Furthermore, the size of the FSS sensor can be scaled up or down as required. Previous work [45] has indicated that even a unit cell is able to produce a transmission response by adjusting the distance of the antennas used for testing.

Fig. 14 shows a potential setup integrated in a wireless sensor network. The sensor is set in such a way that liquids can fall into the FSS structure. To ensure the uniformity of the liquid during the measurements, a bubble level should be used during the installation to prevent erroneous readings. The sensor has a flat surface, which means that some droplets may remain on the surface outside the trenches, which may affect measurements. A future version of the design is envisaged where cells could be three-dimensional with a slight slope to allow droplets to be guided toward the trenches.

Note that this is the first concept and the reading setup is the standard for FSS measurements. However, a more compact arrangement could be developed in the future where the antennas and system only target the specified frequency band of operation. In addition, in an industrial environment, a dedicated space would be desirable.

Even though the main application described here is on liquid sensing, the structure and design have potential applications in reconfigurable FSS using low-loss liquids such as the one employed in [46].

ACKNOWLEDGMENT

The authors would like to thank A. Mendoza for setting up the chamber for measurement and Andrew Brookman for facilitating the fabrication of the milled sensor at Printech Circuit Laboratories Ltd., Chelmsford, U.K.

REFERENCES

[1] A. Ebrahimi, J. Scott, and K. Ghorbani, "Microwave reflective biosensor for glucose level detection in aqueous solutions," *Sens. Actuators A, Phys.*, vol. 301, Jan. 2020, Art. no. 111662.

[2] A. A. M. Bahar, Z. Zakaria, M. K. M. Arshad, A. A. M. Isa, Y. Dasril, and R. A. Alahnomi, "Real time microwave biochemical sensor based on circular SIW approach for aqueous dielectric detection," *Sci. Rep.*, vol. 9, no. 1, pp. 1–12, Dec. 2019.

[3] L. F. Chen, C. K. Ong, C. P. Neo, V. V. Varadan, and V. K. Varadan, *Microwave Electronics Measurements and Materials Characterization*. Chichester, U.K.: Wiley, 2004.

[4] B. A. Galwas, J. K. Piotrowski, and J. Skulski, "Dielectric measurements using a coaxial resonator opened to a waveguide below cut-off," *IEEE Trans. Instrum. Meas.*, vol. 46, no. 2, pp. 511–514, Apr. 1997.

[5] H. Lobato-Morales, A. Corona-Chávez, D. V. B. Murthy, and J. L. Olvera-Cervantes, "Complex permittvity measurements using cavity perturbation technique with substrate integrated waveguide cavities," *Rev. Sci. Instrum.*, vol. 81, pp. 1–4, Jun. 2010.

[6] K. Saeed, R. D. Pollard, and I. C. Hunter, "Substrate integrated waveguide cavity resonators for complex permittivity characterization of materials," *IEEE Trans. Microw. Theory Techn.*, vol. 56, no. 10, pp. 2340–2347, Oct. 2008.

[7] A. A. Abduljabar, D. J. Rowe, A. Porch, and D. A. Barrow, "Novel microwave microfluidic sensor using a microstrip split-ring resonator," *IEEE Trans. Microw. Theory Techn.*, vol. 62, no. 3, pp. 679–688, Mar. 2014.

[8] D. J. Rowe, S. Al-Malki, A. A. Abduljabar, A. Porch, D. A. Barrow, and C. J. Allender, "Improved split-ring resonator for microfluidic sensing," *IEEE Trans. Microw. Theory Techn.*, vol. 62, no. 3, pp. 689–699, Mar. 2014.

[9] E. L. Chuma, Y. Iano, G. Fontgalland, and L. L. B. Roger, "Microwave sensor for liquid dielectric characterization based on metamaterial complementary split ring resonator," *IEEE Sensors J.*, vol. 18, no. 24, pp. 9978–9983, Dec. 2018.

[10] C. Lee, B. Bai, Q. Song, Z. Wang, and G. Li, "Open complementary split-ring resonator sensor for dropping-based liquid dielectric characterization," *IEEE Sensors J.*, vol. 19, no. 24, pp. 11880–11890, Dec. 2019.

[11] A. A. Abduljabar, N. Clark, J. Lees, and A. Porch, "Dual mode microwave microfluidic sensor for temperature variant liquid characterization," *IEEE Trans. Microw. Theory Techn.*, vol. 65, no. 7, pp. 2572–2582, Jul. 2017.

[12] A. J. Cole and P. R. Young, "Chipless liquid sensing using a slotted cylindrical resonator," *IEEE Sensors J.*, vol. 18, no. 1, pp. 149–156, Jan. 2018.

[13] V. Makarovaite, A. J. R. Hillier, S. J. Holder, C. W. Gourlay, and J. C. Batchelor, "Passive wireless UHF RFID antenna label for sensing dielectric properties of aqueous and organic liquids," *IEEE Sensors J.*, vol. 19, no. 11, pp. 4299–4307, Jun. 2019.

[14] S. S. Bukhari, J. Vardaxoglou, and W. Whittow, "A metasurfaces review: Definitions and applications," *Appl. Sci.*, vol. 9, no. 13, pp. 1–14, 2019.

[15] N. Christopoulos, G. Goussetis, A. P. Feresidis, and J. C. Vardaxoglou, "Metamaterials with multiband AMC and EBG properties," in *Proc. Eur. Microw. Conf.*, Paris, France, Oct. 2005, p. 3.

[16] F. Bayatpur and K. Sarabandi, "Tuning performance of metamaterial-based frequency selective surfaces," *IEEE Trans. Antennas Propag.*, vol. 57, no. 2, pp. 590–592, Feb. 2009.

[17] Y. I. Abdulkarim, L. Deng, O. Altıntaş, E. Ünal, and M. Karaaslan, "Metamaterial absorber sensor design by incorporating swastika shaped resonator to determination of the liquid chemicals depending on electrical characteristics," *Phys. E, Low-Dimensional Syst. Nanostruct.*, vol. 114, Oct. 2019, Art. no. 113593.

[18] Y. I. Abdulkarim et al., "Design and study of a metamaterial based sensorfor the application of liquid chemicals detection," *J. Mater. Res. Technol.*, vol. 9, no. 5, pp. 10291–10304, 2020.

[19] Y. I. Abdulkarim et al., "Novel metamaterials-based hypersensitized liquid sensor integrating omega-shaped resonator with microstrip transmission line," *Sensors*, vol. 20, no. 3, pp. 1–18, 2020.

[20] S. Y. Jun., B. S. Izquierdo, and E. A. Parker, "Liquid sensor/detector using an EBG structure," *IEEE Trans. Antennas Propag.*, vol. 67, no. 5, pp. 3366–3373, May 2019.

[21] A. Arif, A. Zubair, K. Riaz, M. Q. Mehmood, and M. Zubair, "A novel cesaro fractal EBG-based sensing platform for dielectric characterization of liquids," *IEEE Trans. Antennas Propag.*, vol. 69, no. 5, pp. 2887–2895, May 2021.

[22] E. A. Parker. (Apr. 17, 1991). *The Gentleman's Guide to Frequency Selective Surfaces*. Accessed: Apr. 27, 2021. [Online]. Available: https://kar.kent.ac.uk/59863/

[23] B. A. Munk, *Frequency Selective Surfaces Theory and Design*. New York, NY, USA: Wiley, 2000.

[24] J. Yiannis and C. Vardaxoglou, "Metamaterial arrays and applications: FSS, EBG & AMC structures," in *Proc. Int. Workshop Antenna Technol., Small Antennas, Novel EM Struct. Mater., Appl. (iWAT)*, Sydney, NSW, Australia, Mar. 2014, p. 269.
[25] F. H. W. Mustaffa, S. N. Azemi, M. F. Jamlos, A. A. Al-Hadi, and P. J. Soh, "Frequency selective surface for structural health monitoring," in *Proc. IOP Conf. Mater. Sci. Eng.*, vol. 318, 2018, pp. 1–9.
[26] D. Pieper, K. M. Donnell, O. Abdelkarim, and M. A. ElGawady, "Embedded FSS sensing for structural health monitoring of bridge columns," in *Proc. IEEE Int. Instrum. Meas. Technol. Conf.*, Taiwan, May 2016, pp. 1–5.
[27] S.-D. Jang, B.-W. Kang, and J. Kim, "Frequency selective surface based passive wireless sensor for structural health monitoring," *Smart Mater. Struct.*, vol. 22, pp. 1–7, Dec. 2013.
[28] M. Mahmoodi and K. M. Donnell, "Novel FSS-based sensor for concurrent temperature and strain sensing," in *Proc. IEEE Int. Symp. Antennas Propag. USNC/URSI Nat. Radio Sci. Meeting*, San Diego, CA, USA, Jul. 2017, pp. 679–680.
[29] S. Milici, J. Lorenzo, A. Lázaro, R. Villarino, and D. Girbau, "Wireless breathing sensor based on wearable modulated frequency selective surface," *IEEE Sensors J.*, vol. 17, no. 5, pp. 1285–1292, Mar. 2017.
[30] S. Soltani, P. S. Taylor, E. A. Parker, and J. C. Batchelor, "Popup tunable frequency selective surfaces for strain sensing," *IEEE Sensors Lett.*, vol. 4, no. 4, pp. 1472–2475, Mar. 2020.
[31] F. Costa, C. Amabile, A. Monorchio, and E. Prati, "Waveguide dielectric permittivity measurement technique based on resonant FSS filters," *IEEE Microw. Wireless Compon. Lett.*, vol. 21, no. 5, pp. 273–275, May 2011.
[32] M. Mahmoodi and K. M. Donnell, "Performance metrics for frequency selective surface-based sensors," *IEEE Sensors Lett.*, vol. 1, no. 6, pp. 1–4, Dec. 2017.
[33] D. Ferreira, R. Caldeirinha, I. Cuiñas, and T. Fernandes, "Square loop and slot frequency selective surfaces study for equivalent circuit model optimization," *IEEE Trans. Antennas Propag.*, vol. 63, no. 9, pp. 3947–3955, Sep. 2015.
[34] R. J. Langley and E. A. Parker, "Equivalent circuit model for arrays of square loops," *Electron. Lett.*, vol. 18, no. 7, pp. 294–296, Apr. 1982.
[35] C. K. Lee and R. J. Langley, "Equivalent-circuit models for frequency-selective surfaces at oblique angles of incidence," *IEE Proc. H-Microw., Antennas Propag.*, vol. 132, no. 6, pp. 395–399, Oct. 1985.
[36] A. Egemen and M. Kuzuoglu, "Design of the square loop frequency selective surfaces with particle swarm optimization via the equivalent circuit model," *Radioengineering*, vol. 18, no. 12, pp. 95–102, Jun. 2009.
[37] N. Marcuvitz, *Waveguide Handbook*. London, U.K.: Peter Peregrinus, 1986.
[38] F. Costa, A. Monorchio, and G. Manara, "Efficient analysis of frequency-selective surfaces by a simple equivalent-circuit model," *IEEE Antennas Propag. Mag.*, vol. 54, no. 4, pp. 35–48, Aug. 2012.
[39] P. Callaghan and E. A. Parker, "Element dependency in dielectric tuning of frequency selective surfaces," *Electron. Lett.*, vol. 28, no. 1, pp. 42–44, Jan. 1992.
[40] A. P. Gregory and R. N. Clarke, "Tables of the complex permittivity of dielectric reference liquids at frequencies up to 5 GHz," Nat. Phys. Lab., Teddington, U.K., NPL Rep. MAT 23, 2012.
[41] CEM. *Solvent Choice for Microwave Synthesis*. Accessed: Jun. 1, 2021. [Online]. Available: https://cem.com/uk/microwave-chemistry/solvent-choice
[42] *Printech Circuit Laboratories*. Accessed: Aug. 20, 2021. [Online]. Available: https://www.pcbs.space/
[43] A. C. de Lima, E. A. Parker, and R. J. Langley, "Tunable frequency selective surface using liquid substrates," *Electron Lett.*, vol. 30, no. 4, pp. 281–282, Feb. 1994.
[44] H. Lobato-Morales, D. V. B. Murthy, A. Corona-Chavez, J. L. Olvera-Cervantes, J. Martínez-Brito, and L. G. Guerrero-Ojeda, "Permittivity measurements at microwave frequencies using epsilon-near-zero (ENZ) tunnel structure," *IEEE Trans. Microw. Theory Techn.*, vol. 59, no. 7, pp. 1863–1868, Jul. 2011.
[45] E. A. Parker, J.-B. Robertson, B. Sanz-Izquierdo, and J. C. Batchelor, "Minimal size FSS for long wavelength," *Electron. Lett.*, vol. 44, no. 6, pp. 394–395, 2008.
[46] C. Song et al., "Passive beam-steering gravitational liquid antennas," *IEEE Trans. Antennas Propag.*, vol. 68, no. 4, pp. 3207–3212, Aug. 2020.

Peter M. Njogu is currently pursuing the Ph.D. degree in electronic engineering with the University of Kent, Canterbury, U.K.

His research interests include wearable antennas, multiband antennas, millimeter-wave antennas, and 3-D printed antennas.

Benito Sanz-Izquierdo received the B.Sc. degree from ULPGC, Las Palmas, Spain, and the M.Sc. and Ph.D. degrees from the University of Kent, Canterbury, U.K.

He was a Research Associate with the School of Engineering, University of Kent, where he became a Lecturer in electronic systems in 2013 and a Senior Lecturer in 2018. In 2012, he worked at Harada Industries Ltd., where he developed novel antennas for the automotive industry. His research interests include multiband antennas, wearable electronics, additive manufacturing (3-D printing), substrate integrated waveguides components, metamaterials, sensors, electromagnetic bandgap structures, frequency-selective surfaces, and reconfigurable devices.

Edward A. Parker (TED) received the M.A. degree in physics and the Ph.D. degree in radio astronomy from the St. Catharine's College, University of Cambridge, Cambridge, U.K, in 1968, respectively.

He was appointed as a Reader with the University of Kent, Canterbury, U.K., in 1977, where he has been a Professor of radio communications since 1987. He is currently a Professor Emeritus with the University of Kent. He established the Electronics Laboratory, Antennas Group, University of Kent. He is a member of the Livery of the Worshipful Company of Scientific Instrument Makers, London, U.K. His current research interests include the application of frequency-selective surfaces and the study and overhaul of antique clocks.

Prof. Parker is a member of the Institution of Engineering and Technology.